Commun. Comput. Phys.
doi: 10.4208/cicp.240815.301215a

Vol. **20**, No. 1, pp. 250-278
July 2016

A Posteriori Error Estimates for Conservative Local Discontinuous Galerkin Methods for the Generalized Korteweg-de Vries Equation

Ohannes Karakashian[1] and Yulong Xing[2,*]

[1] *Department of Mathematics, The University of Tennessee, Knoxville, TN 37996, USA.*
[2] *Department of Mathematics, University of California Riverside, Riverside, CA 92521, USA.*

Communicated by Chi-Wang Shu

Received 24 August 2015; Accepted (in revised version) 30 December 2015

Abstract. We construct and analyze conservative local discontinuous Galerkin (LDG) methods for the Generalized Korteweg-de-Vries equation. LDG methods are designed by writing the equation as a system and performing separate approximations to the spatial derivatives. The main focus is on the development of conservative methods which can preserve discrete versions of the first two invariants of the continuous solution, and a posteriori error estimates for a fully discrete approximation that is based on the idea of dispersive reconstruction. Numerical experiments are provided to verify the theoretical estimates.

AMS subject classifications: 65M12, 65M60, 35Q53

Key words: Discontinuous Galerkin methods, Korteweg-de-Vries equation, a posteriori error estimate, conservative methods.

1 Introduction

In this paper we consider the Generalized Korteweg-de Vries (GKdV) equation posed with periodic boundary conditions

$$\begin{cases} u_t+(u^{p+1})_x+\epsilon u_{xxx}=0, & 0<x<1,\ t>0, \\ u(x,0)=u^0(x), & 0<x<1, \end{cases} \tag{1.1}$$

where p is a positive integer and ϵ is a positive parameter. The GKdV equation belongs to a class of equations featuring nonlinear and dispersive effects that are widely used to model the propagation of physical waves.

*Corresponding author. *Email addresses:* `ohannes@math.utk.edu` (O. Karakashian), `xingy@ucr.edu` (Y. Xing)

Since the discovery of the solitons in the sixties there has been intense interest and resulting research activity on the well-posedness as well as the numerical treatment of (1.1) and other nonlinear dispersive equations. The problem (1.1) is locally well-posed in a wide range of function classes, but it is also known that solutions do not exist for all time and singularity formation may occur, as can be gleaned from [3, 23, 24]. In parallel to the analytical developments, intense attention focused on developing methods for the numerical treatment of (1.1) resulting in schemes belonging to all the known classes of numerical methods including finite difference, finite element, finite volume and spectral methods as well as "special" methods based on the inverse scattering transform. We refer to [9] and the references therein for a survey of such works. However, it must be said that a combination of the nonlinearity and the dispersive term u_{xxx} (which is a derivative of odd order) makes the rigorous treatment of issues such as stability and convergence quite difficult. Whereas a few early works contained such rigorous treatments, the work of Shu and coworkers in the new century on discontinuous Galerkin (DG) methods constituted an important development through the construction of a dissipative dispersive projection operator [11, 27]. In [9] two of the authors advanced the paradigm and showed that a conservative version of the dissipative operator constructed in [11, 27] has beneficial numerical properties such as slower growth of the errors over long time intervals.

As in [9], the numerical methods discussed here are the DG methods. They are characterized by the use of piecewise polynomial spaces that are totally discontinuous, and were originally devised to solve hyperbolic conservation laws with only first order spatial derivatives, e.g. [13–15, 17, 18, 25]. They allow arbitrarily unstructured meshes, and have a compact stencil; moreover, they easily accommodate arbitrary h-p adaptivity. The DG methods were later generalized to the local DG (LDG) methods by Cockburn and Shu to solve the convection-diffusion equation [16], motivated by successful numerical experiments from Bassi and Rebay for the compressible Navier-Stokes equations [6]. As a result, the LDG methods have been applied to solve various partial differential equations (PDEs) containing higher-order derivatives. We refer to the review paper [26] for more details. The LDG method, in contrast to the so-called primitive variable formulations, is characterized by writing the evolution equation as a system by considering each spatial derivative as a dependent variable, one benefit of such an approach being the simultaneous approximation of the spatial derivatives. For the KdV-type equations (1.1), an LDG method was first developed in [29], in which a sub-optimal error estimate was provided for the linearized problem. In [27], Xu and Shu proved the $k+1/2$-th order convergence rate for the LDG method applied to the fully nonlinear KdV equation. Later, an optimal L^2 error estimate was derived in [28] for the linearized equation. Recently, there has been a different approach in solving the KdV equations by using the DG method directly without introducing any auxiliary variables nor rewriting the original equation into a larger system. Cheng and Shu proposed such DG methods in [12] for PDEs involving high-order derivatives, and an energy-conserving DG method for the KdV equation was developed by Bona et al. in [9]. The superconvergence property of the LDG methods for the linearized KdV equation has been studied in [20].

In the present work we focus on two main issues. The first is to extend the conservative approach of [9] to the LDG method. For the linearized KdV equation, we have presented the a priori error estimate, and showed that such conservative methods conserve the first three invariants exactly. The other goal is to develop a posteriori error estimates for the error, i.e., to obtain computable upper bounds on the discretization error of the fully discrete approximations for the LDG method. Such a posteriori error estimates enable the construction of adaptive numerical methods and will be the subject of a forthcoming work. The idea, first described in [21], is to construct a computable function of x and t from the numerical solution, which is smooth enough to satisfy the PDE (1.1) in the strong sense but with a computable forcing term instead of zero. This enables the use of a priori techniques to obtain the bounds on the error.

The paper is organized as follows: Section 2 is devoted to preliminaries and the description of the LDG numerical methods. In particular, the conservative nonlinear and dispersive operators that are necessary for the formulation of the semidiscrete and fully discrete approximations are introduced. In Section 3, conservation properties and optimal error estimates are shown for the semidiscrete formulation of the linearized problem. In Section 4, a conservative reconstruction operator, which is different from the one in [21], is introduced and is used to obtain an a posteriori error estimate for the semidiscrete formulation (2.28)-(2.30). The a posteriori error estimation for a fully discrete scheme based on the Backward Euler method is then derived. The technique consists in using a second, more accurate scheme based on the midpoint rule, to obtain the computable error bounds. This approach is similar to the long-standing technique used in adaptive algorithms for initial value problems for ordinary differential equations, with the essential difference that rigorous error bounds have been obtained. Finally, in Section 5, results of numerical experiments are reported concerning the performance of the algorithms in the light of both the a priori and a posteriori theoretical estimates.

2 The numerical approximation

In this section, we present the details of the numerical approximations. This begins with a discussion of the notations and spatial discretization which lead directly to a semidiscrete approximation of the continuous problem.

2.1 The meshes

Let $\mathcal{T}_h$ denote a partition of the domain $[0,1]$ which has the form $0=x_0<x_1<\cdots<x_M=1$. These points x_m are called *nodes* while the intervals $I_m=[x_m,x_{m+1}]$ will be referred to as *cells*. The notation $x_m^-=x_m^+=x_m$ will be useful in taking account, respectively, of left- and right-hand limits of discontinuous functions. Corresponding to the underlying spatial periodicity of the solutions being approximated, we have taken $x_0^-=x_M^-$ and $x_M^+=x_0^+$. The meshes $\mathcal{T}_h$ are assumed to be *quasi-uniform*, which means that if $h_m=x_{m+1}-x_m$ and

$h = h_{\max} = \max_m h_m$, then there is a positive constant c such that, for all m,

$$0 < c \leq \frac{h_m}{h}. \tag{2.1}$$

2.2 Function spaces

In addition to the usual Sobolev spaces $W^{s,p} = W^{s,p}([0,1])$, we will repeatedly use use the so-called *broken* Sobolev spaces $W^{s,p}(\mathcal{T}_h)$, which are the finite Cartesian products $\Pi_{I\in\mathcal{T}_h} W^{s,p}(I)$. Note that if $sp > 1$, the elements of $W^{s,p}(\mathcal{T}_h)$ are uniformly continuous when restricted to a given cell, but they may be discontinuous across nodes. To quantify these potential discontinuities, we introduce the following notation: for $v \in W^{s,p}(\mathcal{T}_h), s \geq 1$, let v_m^+ and v_m^- denote the right-hand and left-hand limits, respectively, of v at the node x_m. We adopt the standard notations in the context of DG-methods. the *jump* $[v_m]$ of v at x_m is defined as $v_m^+ - v_m^-$, and the *average* $\{v_m\}$ of v at x_m is $\frac{1}{2}(v_m^+ + v_m^-)$. In all cases, the definitions are meant to adhere to the convention that $v_0^- = v_M^-$ and $v_M^+ = v_0^+$.

Norms in the Sobolev classes $W^{s,p}$ will be denoted $\|\cdot\|_{W^{s,p}}$ or $\|\cdot\|_{W^{s,p}(I)}$ when the interval I might be in doubt. In case the interval I is clear from context, we will sometimes use an unadorned norm $\|\cdot\|$ to connote the $L^2(I)$-norm. We also introduce the classes $L^p([0,T];W^{s,r})$ of functions $u = u(x,t)$ which are measurable mappings from $[0,T]$ into $W^{s,r}$ and such that

$$\|u\|_{L^p([0,T];W^{s,r})} = \left(\int_0^T \|u(\cdot,\tau)\|_{W^{s,r}}^p \, d\tau \right)^{1/p} < \infty,$$

with the usual modification if $p = \infty$.

The following embedding inequality (see [1]) will find frequent use in our analysis. For $v \in H^1(\mathcal{T}_h) = W^{1,2}(\mathcal{T}_h)$ and any cell $I \in \mathcal{T}_h$, there is a constant c which is independent of the cell I such that

$$\|v\|_{L^\infty(I)} \leq c \left(h_I^{-1/2} \|v\|_{L^2(I)} + h_I^{1/2} \|v_x\|_{L^2(I)} \right), \tag{2.2}$$

where h_I is the length of I. Note that (2.2) may also be viewed as a trace inequality.

2.3 The discontinuous polynomial spaces

The spatial numerical approximations will be sought in the space of discontinuous, piecewise polynomial functions V_h^q subordinate to the mesh $\mathcal{T}_h$, which is defined by

$$V_h^q = \{v : v\big|_{I_m} \in \mathcal{P}_q(I_m),\ m = 1,\cdots,M\}.$$

Here $\mathcal{P}_q$ is the space of polynomials of degree q. The spaces V_h^q have well known, local approximation and inverse properties which are spelled out here for convenience (cf. [5],

[10]). Let q be fixed and let i,j be such that $0\le j\le i\le q+1$. Then, for any cell I and any v in $H^j(I)$, there exists a $\chi\in\mathcal{P}_q(I)$ such that

$$|v-\chi|_{j,I}\le ch_I^{i-j}|v|_{i,I}, \tag{2.3}$$

where $|v|_{i,I}$ denotes the seminorm $\|v^{(i)}\|_{L^2(I)}$ on the Sobolev space $H^i(I)$ and the constant c is independent of h_I. The above property continues to hold if the L^p-based Sobolev spaces replace the L^2-based classes H^j. In particular, it holds for the L^∞ norm, which is to say, with i,j as above, there is a $\chi\in\mathcal{P}_q(I)$ such that

$$|\partial_x^j(v-\chi)|_{L^\infty(I)}\le ch_I^{i-j}|\partial_x^i v|_{L^\infty(I)}. \tag{2.4}$$

The equally well-known inverse inequality is given by

$$|\chi|_{j,I}\le ch_I^{-j}|\chi|_{0,I}, \tag{2.5}$$

for all $\chi\in\mathcal{P}_q(I)$ (see [10]).

2.4 The weak formulation

It is well-known that the first step for formulating an LDG method is to rewrite the given PDE as a first order system by introducing auxiliary variables. For the GKDV equation (1.1), we have

$$\begin{aligned} u_t+(u^{p+1})_x+\epsilon w_x&=0, \qquad (x,t)\in[0,1]\times(0,T], && (2.6)\\ w&=v_x, \qquad (x,t)\in[0,1]\times[0,T], && (2.7)\\ v&=u_x, \qquad (x,t)\in[0,1]\times[0,T]. && (2.8)\end{aligned}$$

Multiplying (2.6)-(2.8) by test functions ϕ, ψ and φ in $H^1(\mathcal{T}_h)$ and integrating by parts, we see that the above equations can be written as

$$\sum_{I\in\mathcal{T}_h}(u_t,\phi)_I-\sum_{I\in\mathcal{T}_h}(u^{p+1},\phi_x)_I-\sum_{m=0}^{M-1}u_m^{p+1}[\phi]_m-\sum_{I\in\mathcal{T}_h}\epsilon(w,\phi_x)_I-\sum_{m=0}^{M-1}\epsilon w_m[\phi]_m=0, \tag{2.9}$$

$$\sum_{I\in\mathcal{T}_h}(w,\psi)_I=-\sum_{I\in\mathcal{T}_h}(v,\psi_x)_I-\sum_{m=0}^{M-1}v_m[\psi]_m, \tag{2.10}$$

$$\sum_{I\in\mathcal{T}_h}(v,\varphi)_I=-\sum_{I\in\mathcal{T}_h}(u,\varphi_x)_I-\sum_{m=0}^{M-1}u_m[\varphi]_m, \tag{2.11}$$

using the fact that u,v,w are smooth, where $(\cdot,\cdot)$ denotes the L^2 inner product, that is, $(f,g)_I=\int_I fg\,dx$ and $(f,g)=\int_0^1 fgdx$.

As done in the construction of DG methods, we shall replace the u,v,w terms in the four "jump" terms that appeared during the process of integration by parts by appropriate *flux* terms that ensure correct transmission of information across the cells when u,v and w are replaced by discontinuous functions. Furthermore, our specific choices are also guided by the desire to construct conservative schemes in a sense that will be made precise shortly.

For the nonlinear jump term, we consider the "flux"

$$u_m^{p+1} \leftarrow (\widehat{u^{p+1}})_m := \frac{1}{p+2} \sum_{j=0}^{p+1} (u_m^+)^{p+1-j} (u_m^-)^j, \tag{2.12}$$

and define the nonlinear form $\mathcal{N} : H^1(\mathcal{T}_h) \times H^1(\mathcal{T}_h) \to R$ by

$$\mathcal{N}(u,\phi) = -\sum_{I\in\mathcal{T}_h} (u^{p+1},\phi_x)_I - \sum_{m=0}^{M-1} (\widehat{u^{p+1}})_m [\phi_m]. \tag{2.13}$$

For the terms u_m,v_m and w_m in the remaining three jump terms, we define the fluxes by

$$u_m \leftarrow \hat{u}_m := \{u\}_m, \quad v_m \leftarrow \hat{v}_m := \{v\}_m, \quad w_m \leftarrow \hat{w}_m := \{w\}_m,$$

and the corresponding bilinear form $\mathcal{D} : H^1(\mathcal{T}_h) \times H^1(\mathcal{T}_h) \to R$ by

$$\mathcal{D}(s,\psi) = -\sum_{I\in\mathcal{T}_h} (s,\phi_x)_I - \sum_{m=0}^{M-1} \{s\}_m [\phi]_m. \tag{2.14}$$

With the forms $\mathcal{N}$ and $\mathcal{D}$ at hand, the weak formulation of (2.6)-(2.8) can be expressed as

$$(u_t,\phi) + \mathcal{N}(u,\phi) + \epsilon\mathcal{D}(w,\phi) = 0, \quad \forall \phi \in H^1(\mathcal{T}_h), \tag{2.15}$$

$$(w,\psi) = \mathcal{D}(v,\psi), \quad \forall \psi \in H^1(\mathcal{T}_h), \tag{2.16}$$

$$(v,\varphi) = \mathcal{D}(u,\varphi), \quad \forall \varphi \in H^1(\mathcal{T}_h). \tag{2.17}$$

Next, we exhibit some properties of the forms introduced above.

Lemma 2.1. *The form $\mathcal{N}$ defined by* (2.13) *is:*

(i) consistent in the sense that for all $u \in C^1[0,1]$ (periodicity is included in the definition of $C^1[0,1]$), there holds

$$\mathcal{N}(u,\phi) = ((u^{p+1})_x,\phi), \quad \forall\, \phi \in H^1(\mathcal{T}_h); \tag{2.18}$$

(ii) conservative in the sense that

$$\mathcal{N}(\phi,\phi) = 0, \quad \forall\, \phi \in H^1(\mathcal{T}_h). \tag{2.19}$$

Using the Riesz Representation Theorem, we can define the nonlinear operator $\mathcal{N}: H^1(\mathcal{T}_h)\to V_h^q$ via

$$(\mathcal{N}(u),\phi)=\mathcal{N}(u,\phi), \quad \forall\phi\in V_h^q. \tag{2.20}$$

For the bilinear form $\mathcal{D}$, we see that it possesses the following skew-adjointness property.

Lemma 2.2. *The form $\mathcal{D}$ defined by* (2.14) *satisfies*

$$\mathcal{D}(\phi,\psi)=-\mathcal{D}(\psi,\phi), \quad \forall\ \phi,\psi\in H^1(\mathcal{T}_h), \quad \text{and thus} \quad \mathcal{D}(\phi,\phi)=0, \quad \forall\ \phi\in H^1(\mathcal{T}_h). \tag{2.21}$$

Proof. Using the definition of $\mathcal{D}$, integration by parts and the identity $[\phi\psi]_m=\{\phi\}_m[\psi]_m+[\phi]_m\{\psi\}_m$, we obtain

$$\begin{aligned}\mathcal{D}(\phi,\psi)&=-\sum_{I\in\mathcal{T}_h}(\phi,\psi_x)_I-\sum_{m=0}^{M-1}\{\phi\}_m[\psi]_m\\&=\sum_{I\in\mathcal{T}_h}(\phi_x,\psi)_I+\sum_{m=0}^{M-1}[\phi\psi]_m-\sum_{m=0}^{M-1}\{\phi\}_m[\psi]_m=-\mathcal{D}(\psi,\phi).\end{aligned}$$

The fact that $\mathcal{D}(\phi,\phi)=0$ is now an easy consequence. □

We may also define the linear operator $\mathcal{D}: H^1(\mathcal{T}_h)\to V_h^q$ by

$$(\mathcal{D}(u),\phi)=\mathcal{D}(u,\phi), \quad \forall\phi\in V_h^q. \tag{2.22}$$

The bilinear form $\mathcal{D}$ and thus the associated linear operator corresponds to a discrete version of the first-order differentiation operator. Indeed, we have

Lemma 2.3. *Let $u\in C^0[0,1]\cap H^1(\mathcal{T}_h)$. Then,*

$$\mathcal{D}(u,\phi)=(u_x,\phi), \quad \forall\ \phi\in H^1(\mathcal{T}_h). \tag{2.23}$$

In operator form, this can be expressed as

$$\mathcal{D}u=P_0u_x, \tag{2.24}$$

where $P_0: L^2(0,1)\to V_h^q$ is the L^2 projection operator into V_h^q.

Proof. Using integration by parts in (2.14) and the identity $[u\phi]_m=\{u\}_m[\phi]_m+[u]_m\{\phi\}_m$, we arrive at

$$\mathcal{D}(u,\phi)=\sum_{I\in\mathcal{T}_h}(u_x,\phi)_I+\sum_{m=0}^{M-1}[u]_m\{\phi\}_m, \quad \forall\ \phi\in H^1(\mathcal{T}_h).$$

Since u is continuous and also periodic, the jumps $[u]_m$ vanish. Now it is easily shown that $u\in H^1(0,1)$. Hence, it follows that $\mathcal{D}(u,\phi)=\sum_{I\in\mathcal{T}_h}(u_x,\phi)_I=(u_x,\phi)$, establishing (2.23). To prove (2.24), it suffices to observe that $(\mathcal{D}u,\phi)=\mathcal{D}(u,\phi)=(u_x,\phi)$, $\forall\ \phi\in V_h^q$. □

Remark 2.1. It is clear from the discussion above and in particular (2.21) and (2.24) that $(\mathcal{D}u,u)=0$. This is a discrete version of the fact that $(u_x,u)=0$ for smooth and periodic u and motivates calling the operator $\mathcal{D}$ conservative since it preserves a property that holds at the continuous level.

As an immediate consequence of the preceding lemma we have

Lemma 2.4. *(i) The form $\mathcal{D}$ defined by* (2.14) *is consistent in the sense that for $u\in C^2[0,1]\cap H^3(\mathcal{T}_h)$ and $w=u_{xx}$, there holds*

$$\mathcal{D}(w,\phi)=(u_{xxx},\phi),\quad \forall\,\phi\in H^1(\mathcal{T}_h). \tag{2.25}$$

(ii) The form $\mathcal{D}$ defined by (2.14) *is conservative in the sense that for any $u\in H^1(\mathcal{T}_h)$ there holds*

$$\mathcal{D}(w,u)=0\quad where\quad w,v\in V_h^q\quad are\ given\ by\quad w=\mathcal{D}v,\ v=\mathcal{D}u. \tag{2.26}$$

Proof. It is clear that u_{xx} belongs to $C^0[0,1]\cap H^1(\mathcal{T}_h)$; therefore (2.25) follows readily from (2.23). As for (ii), we have

$$\begin{aligned}\mathcal{D}(w,u)&=\mathcal{D}(\mathcal{D}\mathcal{D}u,u)=-\mathcal{D}(u,\mathcal{D}\mathcal{D}u)=-(\mathcal{D}u,\mathcal{D}\mathcal{D}u)\\&=-(\mathcal{D}\mathcal{D}u,\mathcal{D}u)=-\mathcal{D}(\mathcal{D}u,\mathcal{D}u)=0\end{aligned} \tag{2.27}$$

using the skew-adjointness property (2.21). □

With the operators $\mathcal{N}$ and $\mathcal{D}$, we can now introduce a semidiscrete LDG formulation for the problem (1.1) expressed as the system (2.6)-(2.8): we define $u_h,v_h,w_h:[0,T]\to V_h^q$, the semidiscrete approximation of u,u_x,u_{xx}, respectively by

$$u_{ht}+\mathcal{N}(u_h)+\mathcal{D}w_h=0,\qquad 0<t, \tag{2.28}$$

$$w_h=\mathcal{D}v_h,\quad 0<t, \tag{2.29}$$

$$v_h=\mathcal{D}u_h.\quad 0<t, \tag{2.30}$$

with initial data u_h^0,v_h^0,w_h^0 approximating u^0,u_x^0,u_{xx}^0 respectively and satisfying, in addition, the following compatibility conditions.

$$v_h^0=\mathcal{D}u_h^0,\quad w_h^0=\mathcal{D}v_h^0. \tag{2.31}$$

Remark 2.2. The two relations (conditions) $w_h^0=\mathcal{D}v_h^0$ and $v_h^0=\mathcal{D}u_h^0$ in (2.31) are the compatibility conditions implied by (2.29) and (2.30) as $t\to 0^+$. These compatibility conditions are unavoidable and appear in the proof of error estimates. However, this leads to the difficulty of generating initial approximations which must satisfy these constraints and which at the same time must be optimal order approximations for all three variables. This is indeed a problem for LDG type methods that does not exist for primitive variable formulations. A general procedure for constructing such initial approximations has been devised and will be the subject of a forthcoming work [22].

Theorem 2.1. *Suppose there exist initial approximations satisfying* (2.31). *Then, there exists a unique solution* u_h,v_h,w_h *to the system* (2.28)-(2.30). *Furthermore,* u_h *has the two discrete conservation properties*

$$(u_h(t),1)=(u_h^0,1), \quad \|u_h(t)\|=\|u_h^0\|, \quad t\geq 0. \tag{2.32}$$

Proof. The system (2.28)-(2.30) can be written in the equivalent form

$$u_{ht}+\mathcal{N}(u_h)+\epsilon\mathcal{D}^3 u_h=0, \quad t>0, \quad u_h(0)=u_h^0. \tag{2.33}$$

Since V_h^q is finite dimensional, $\mathcal{N},\mathcal{D}$ are continuous as operators on V_h^q. To show that a unique global in time solution exists, it suffices to produce the a priori bound $\|u_h(t)\|_\infty\leq c$, $t\geq 0$. Indeed, multiplying (2.33) by u_h, integrating over $[0,1]$ with respect to x and using (2.29), we obtain

$$\frac{1}{2}\frac{d}{dt}\|u_h(t)\|^2+\mathcal{N}(u_h,u_h)+\epsilon\mathcal{D}(w_h,u_h)=0.$$

Note that in view of (2.19) and (2.26) we have $\mathcal{N}(u_h,u_h)=0$ and $\mathcal{D}(w_h,u_h)=0$. Thus $\|u_h(t)\|=\|u_h^0\|$, establishing the second conservation law in (2.32). Since all norms on V_h^q are equivalent, it follows that $\|u_h\|_{L^\infty}$ is bounded for all $t\geq 0$ by a constant that may depend on the dimension of V_h^q. Finally, the first conservation law of (2.32) is a consequence of the fact that $\mathcal{N}(\cdot,1)=\mathcal{D}(\cdot,1)=0$. This concludes the proof. $\square$

3 A priori error estimates

For parabolic and hyperbolic equations, a crucial tool in deriving error estimates has been the so-called *Elliptic Projection* of the solution u. Since differential operators of odd order lack the positivity property of $-\Delta$, devising an appropriate projection for them turns out to be much more arduous.

We construct a projection operator $\mathcal{P}:H^1(\mathcal{T}_h)\to V_h^q$ as follows

$$\begin{aligned} &(\mathcal{P}u,v)_I=(u,v)_I, && \forall v\in\mathcal{P}_{q-1}(I),\ I\in\mathcal{T}_h,\\ &\{\mathcal{P}u\}_m=\{u\}_m, && m=0,\cdots,M-1. \end{aligned} \tag{3.1}$$

The operator $\mathcal{P}$ is related to the first-order conservative derivative operator $\mathcal{D}$ through

$$\mathcal{D}\mathcal{P}u=\mathcal{D}u, \quad \forall u\in H^1(\mathcal{T}_h). \tag{3.2}$$

In view of this relationship, we refer to $\mathcal{P}$ as a conservative projection operator.

To put things in perspective, $\mathcal{P}$ is the analog of the projection operator, which we denote here by $\mathcal{P}^+$, used in [29] and defined by

$$\begin{aligned} &(\mathcal{P}^+u,v)_I=(u,v)_I, && \forall v\in\mathcal{P}_{q-1}(I),\ I\in\mathcal{T}_h,\\ &(\mathcal{P}^+u)_m=u_m^+, && m=0,\cdots,M-1. \end{aligned} \tag{3.3}$$

Indeed, the operator $\mathcal{P}^+$ is related through the identity $\mathcal{D}^+\mathcal{P}^+u=\mathcal{D}^+u$ to the first-order derivative operator $\mathcal{D}^+:H^1(\mathcal{T}_h)\to V_h^q$ defined by

$$(\mathcal{D}^+u,v):=-\sum_{I\in\mathcal{T}_h}(u,v_x)_I-\sum_{m=0}^{M-1}u_m^+[v]_m.$$

Furthermore, it is easily proved that $(\mathcal{D}^+v,v)=-\frac{1}{2}\sum_{m=0}^{M-1}|[v]_m|^2,\quad \forall v\in H^1(\mathcal{T}_h)$. In view of the fact that $(\mathcal{D}^+v,v)$ is negative, we label both operators $\mathcal{D}^+$ and $\mathcal{P}^+$ (the latter solely by association) as dissipative.

In contrast to $\mathcal{P}^+$, the operator $\mathcal{P}$ is global in its definition, due to the coupling across cells including the two endpoints. As a consequence, the analysis of its properties including existence, uniqueness and approximation properties are nontrivial and require certain conditions which are spelled out in the next theorem.

Theorem 3.1. *Suppose u is sufficiently smooth and periodic. Further assume that $q\geq 0$ is even and that the number of cells in $\mathcal{T}_h$ is odd. Then, the operator $\mathcal{P}$ is well-defined and possesses the following approximation properties: For $j=0,1$ and $p=2,\infty$, there holds*

$$\begin{aligned}\|u-\mathcal{P}u\|_{W^{j,p}(I)}&\leq ch_I^{1-j}\left(\sum_{I\in\mathcal{T}_h^N}h_I^q\|u\|_{W^{q+1,\infty}(I)}+\sum_{I\in\mathcal{T}_h\setminus\mathcal{T}_h^N}h_I^{q+1}\|u\|_{W^{q+2,\infty}(I)}\right),\\&\equiv\mathcal{E}(u,q,h,j,p),\end{aligned}\tag{3.4}$$

for a constant c independent of I, where $\mathcal{T}_h^N$ is the set of cells whose length differs from at least one of its two immediate neighbors.

The proof is rather lengthy and is omitted here since it follows the development along the lines of Propositions 3.1 and 3.2 of [9].

Remark 3.1. In general, the cardinality $\#\{\mathcal{T}_h^N\}$ can be as large as M, in which case the estimate (3.4) is $\mathcal{O}(h^q)$ and is quasi optimal. For a uniform mesh, $\#\{\mathcal{T}_h^N\}=0$ and yields the optimal estimate $\mathcal{O}(h^{q+1})$. Between these two extremes, it is possible to achieve extreme local refinements while at the same time keeping $\#\{\mathcal{T}_h^N\}$ quite small. This can be accomplished by implementing refinement in "patches", by which we mean a refinement wherein various subsets of contiguous cells are refined uniformly. This scheme of refinement is very well suited to the simulation of localized singularities.

Remark 3.2. Numerically, we can observe the optimal convergence rate when the polynomial order q is even, and sub-optimal convergence rate for odd q. We have tried various different approaches to derive a priori error estimate of the conservative LDG method for the nonlinear problem, and the best we can obtain is the $(q-1/2)$-th convergence. The main difficulty lies in the combination of the nonlinear term and the choice of conservative numerical fluxes for the dispersive term. Below we show the proof of the optimal convergence for the linearized equation.

3.1 A priori error estimates and conservative properties for the linearized equation

For the linearized equation $u_t+u_x+\epsilon u_{xxx}=0$, we have the following numerical method

$$u_{ht}+\mathcal{D}u_h+\epsilon\mathcal{D}w_h=0, \tag{3.5}$$

$$w_h=\mathcal{D}v_h, \tag{3.6}$$

$$v_h=\mathcal{D}u_h. \tag{3.7}$$

Theorem 3.2. *Let u_h,v_h,w_h be the numerical solutions of the semi-discrete LDG methods* (3.5)-(3.7). *In addition to the two discrete conservation properties* (2.32), *we have*

$$\|v_h(t)\|=\|v_h^0\|,\quad \|w_h(t)\|=\|w_h^0\|,\quad t\geq 0. \tag{3.8}$$

Moreover, the first three invariants of the linearized KdV equation, given by:

$$I_1=\int u dx,\quad I_2=\int u^2 dx,\quad I_3=\int (\epsilon u_x^2-u^2)dx, \tag{3.9}$$

are conserved by the solutions of the LDG methods (3.5)-(3.7).

Proof. First, taking the time derivative of (3.7), using the test functions $-w_h,(u_h)_t,v_h$ in (3.5)-(3.7) and summing them, we obtain

$$\frac{1}{2}\frac{d}{dt}\|v_h\|^2-(\mathcal{D}u_h,w_h)=0, \tag{3.10}$$

where we have also used the skew-symmetry property (2.21) of the operator $\mathcal{D}$. Using the test functions v_h and w_h in (3.6) and (3.7), respectively, and subtracting, we obtain $(\mathcal{D}u_h,w_h)=(\mathcal{D}v_h,v_h)=0$. Therefore, it follows that $\frac{d}{dt}\|v_h\|^2=0$, which leads to the conservation of the L^2 norm of v_h in time.

Taking time derivatives in (3.6) and (3.7), using the test functions $-(v_h)_t,\epsilon w_h,(u_h)_t$ and summing them, we obtain

$$\frac{\epsilon}{2}\frac{d}{dt}\|w_h\|^2-(\mathcal{D}u_h,(v_h)_t)=0.$$

From (3.7), we have $(\mathcal{D}u_h,(v_h)_t)=(v_h,(v_h)_t)$, therefore,

$$\frac{\epsilon}{2}\frac{d}{dt}\|w_h\|^2-\frac{1}{2}\frac{d}{dt}\|v_h\|^2=0,$$

which leads to the conservation of the L^2 norm of w_h in time. The conservation of the three invariants I_1, I_2 and I_3 is a straightforward extension. $\square$

Theorem 3.3. *Assume that the solution u of the linearized equation is sufficiently smooth and periodic. Also, assume that $q\geq 0$ is even, the number of cells in $\mathcal{T}_h$ is odd, and there exist initial approximations u_h^0,v_h^0,w_h^0 satisfying the compatibility conditions* (2.31) *and the optimality conditions*

$$\|u^0-u_h^0\|+\|u_x^0-v_h^0\|+\epsilon\|u_{xx}^0-w_h^0\|=\mathcal{O}(h^{q+1}). \tag{3.11}$$

Then, there holds the estimate

$$\begin{aligned}&\|u(t)-u_h(t)\|+\|u_x(t)-v_h(t)\|+\epsilon\|u_{xx}(t)-w_h(t)\|\\ \leq& ce^{ct}\max_{\substack{k=0,1;\ell=0,1,2\\0\leq s\leq t}}\mathcal{E}(\partial_t^k\partial_x^\ell u(s),q,h,0,2),\end{aligned} \tag{3.12}$$

where the quantity $\mathcal{E}$ is defined in (3.4).

Proof. Let P_0 denote the standard L^2 projection. Applying P_0 to the system (2.6)-(2.8) (without the nonlinear term), using (2.24) and (3.2), we arrive at the system

$$(\mathcal{P}u)_t+\mathcal{D}\mathcal{P}u+\epsilon\mathcal{D}\mathcal{P}w=-P_0\eta_t^{(u)}, \tag{3.13}$$

$$\mathcal{P}w=\mathcal{D}\mathcal{P}v-P_0\eta^{(w)}, \tag{3.14}$$

$$\mathcal{P}v=\mathcal{D}\mathcal{P}u-P_0\eta^{(v)}, \tag{3.15}$$

with the *consistency* terms $\eta^{(u)},\eta^{(v)},\eta^{(w)}$ given by

$$\eta^{(u)}=u-\mathcal{P}u,\quad \eta^{(v)}=v-\mathcal{P}v,\quad \eta^{(w)}=w-\mathcal{P}w.$$

Subtracting each term in (3.13)-(3.15) from the corresponding term in (3.5)-(3.7), we obtain the system

$$\zeta_t^{(u)}+\mathcal{D}\zeta^{(u)}+\epsilon\mathcal{D}\zeta^{(w)}=P_0\eta_t^{(u)}, \tag{3.16}$$

$$\zeta^{(w)}=\mathcal{D}\zeta^{(v)}+P_0\eta^{(w)}, \tag{3.17}$$

$$\zeta^{(v)}=\mathcal{D}\zeta^{(u)}+P_0\eta^{(v)}, \tag{3.18}$$

for the error terms

$$\zeta^{(u)}=u_h-\mathcal{P}u,\quad \zeta^{(v)}=v_h-\mathcal{P}v,\quad \zeta^{(w)}=w_h-\mathcal{P}w.$$

Using the test functions $\zeta^{(u)},\zeta^{(v)},-\zeta^{(w)}$ in (3.16)-(3.18), we obtain after summing

$$\frac{1}{2}\frac{d}{dt}\|\zeta^{(u)}\|^2=(\eta_t^{(u)},\zeta^{(u)})+(\eta^{(w)},\zeta^{(v)})-(\eta^{(v)},\zeta^{(w)}). \tag{3.19}$$

We can use Gronwall's inequality on the term $\zeta^{(u)}$, however, this requires estimates for the terms $\zeta^{(v)}$ and $\zeta^{(w)}$. Taking time derivatives in (3.17) and (3.18), using the test functions $-\zeta_t^{(v)},\epsilon\zeta^{(w)},\zeta_t^{(u)}$, we obtain

$$\frac{\epsilon}{2}\frac{d}{dt}\|\zeta^{(w)}\|^2-(\mathcal{D}\zeta^{(u)},\zeta_t^{(v)})=\epsilon(\eta_t^{(w)},\zeta^{(w)})+(\eta_t^{(v)},\zeta_t^{(u)})-(\eta_t^{(u)},\zeta_t^{(v)}).$$

From (3.18) we readily obtain $(\mathcal{D}\zeta^{(u)},\zeta_t^{(v)})=\frac{1}{2}\frac{d}{dt}\|\zeta^{(v)}\|^2-(\eta^{(v)},\zeta_t^{(v)})$. Using this in the above, we get

$$\frac{\epsilon}{2}\frac{d}{dt}\|\zeta^{(w)}\|^2-\frac{1}{2}\frac{d}{dt}\|\zeta^{(v)}\|^2=\epsilon(\eta_t^{(w)},\zeta^{(w)})+(\eta_t^{(v)},\zeta_t^{(u)})-(\eta_t^{(u)},\zeta_t^{(v)})-(\eta^{(v)},\zeta_t^{(v)}). \tag{3.20}$$

Now, taking the time derivative of (3.18), using the test functions $0,\zeta_t^{(u)},\zeta^{(v)}$, we obtain

$$\frac{1}{2}\frac{d}{dt}\|\zeta^{(v)}\|^2=-(\zeta^{(w)},\zeta_t^{(u)})+(\eta^{(w)},\zeta_t^{(u)})+(\eta_t^{(v)},\zeta^{(v)}).$$

Note that from (3.16) we have $\zeta_t^{(u)}=-\mathcal{D}\zeta^{(u)}-\epsilon\mathcal{D}\zeta^{(w)}+P_0\eta_t^{(u)}$. Using this in the first term on the right side of the above identity, it follows from (2.21) that

$$\frac{1}{2}\frac{d}{dt}\|\zeta^{(v)}\|^2=(\zeta^{(w)},\mathcal{D}\zeta^{(u)})+(\eta_t^{(v)},\zeta^{(v)})-(\eta_t^{(u)},\zeta^{(w)})+(\eta^{(w)},\zeta_t^{(u)}). \tag{3.21}$$

Using the test functions $\zeta^{(v)}$ and $\zeta^{(w)}$ with (3.17) and (3.18), respectively, and subtracting, we see that $(\zeta^{(w)},\mathcal{D}\zeta^{(u)})=(\eta^{(w)},\zeta^{(v)})-(\eta^{(v)},\zeta^{(w)})$. Using this in (3.21), it follows that

$$\frac{1}{2}\frac{d}{dt}\|\zeta^{(v)}\|^2=(\eta^{(w)},\zeta^{(v)})-(\eta^{(v)},\zeta^{(w)})+(\eta_t^{(v)},\zeta^{(v)})-(\eta_t^{(u)},\zeta^{(w)})+(\eta^{(w)},\zeta_t^{(u)}). \tag{3.22}$$

We next multiply (3.22) by 2 and add to the sum of (3.19) and (3.20). This yields

$$\frac{1}{2}\frac{d}{dt}\left(\|\zeta^{(u)}\|^2+\|\zeta^{(v)}\|^2+\epsilon\|\zeta^{(w)}\|^2\right)=(A,\zeta^{(u)})+(B,\zeta^{(v)})+(C,\zeta^{(w)})+(D,\zeta_t^{(u)})+(E,\zeta_t^{(v)}), \tag{3.23}$$

where the time dependent quantities A,B,C,D,E are given by

$$\begin{aligned}&A=\eta_t^{(u)},\quad B=2\eta_t^{(v)}+3\eta^{(w)},\quad C=-3\eta^{(v)}+\epsilon\eta_t^{(w)}-2\eta_t^{(u)},\\&D=\eta_t^{(v)}+2\eta^{(w)},\quad E=-\eta^{(v)}-\eta_t^{(u)}.\end{aligned}$$

We shall apply integration over $[0,t]$ to (3.23). As a preliminary step, we see that integration by parts applied to the last two terms of (3.23) yields

$$\int_0^t(D,\zeta_t^{(u)})ds=(D(t),\zeta^{(u)}(t))-(D(0),\zeta^{(u)}(0))-\int_0^t(D_t,\zeta^{(u)})ds, \tag{3.24}$$

$$\int_0^t(E,\zeta_t^{(v)})ds=(E(t),\zeta^{(v)}(t))-(E(0),\zeta^{(v)}(0))-\int_0^t(E_t,\zeta^{(v)})ds. \tag{3.25}$$

Introducing the quantity $Q(t):=\|\zeta^{(u)}\|^2+\|\zeta^{(v)}\|^2+\epsilon\|\zeta^{(w)}\|^2$, it follows from (3.23)-(3.25), the Cauchy-Schwarz and arithmetic-geometric mean inequalities, that for any $\delta>0$,

$$Q(t)\le Q(0)+\delta Q(t)+\int_0^t Q(s)ds+K, \tag{3.26}$$

where

$$K=\|D(0)\|^2+\|E(0)\|^2+\frac{1}{\delta}\Big(\|D(t)\|^2+\|E(t)\|^2\Big)$$
$$+\int_0^t\Big(\|A\|^2+\|B\|^2+\frac{1}{\epsilon}\|C\|^2+\|D_t\|^2+\|E_t\|^2\Big)ds.$$

Choosing $\delta=1/2$, Gronwall's inequality applied to (3.26) yields

$$Q(t)\le ce^{2t}\big(Q(0)+K\big),\quad t\ge 0. \tag{3.27}$$

Note that $Q(0)=\mathcal{O}(h^{q+1})$ by (3.11). Furthermore, K is defined in terms of $\eta^{(u)},\eta^{(v)},\eta^{(w)}$ and their time derivatives and therefore is bounded by

$$\max_{0\le s\le t}\max_{k=0,1;\ell=0,1,2}\mathcal{E}(\partial_t^k\partial_x^\ell u(s),q,h,0,2)$$

in view of (3.4). Hence, $Q(t)$ is also bounded by the right side of (3.12). Finally, the estimate (3.12) follows from this fact and the triangle inequality. $\square$

4 A posteriori error estimates

Our approach to a posteriori error estimation is based on the idea of reconstruction which is displayed in the following result.

Theorem 4.1. *For $q\ge 2$, there exists a unique reconstruction operator $\mathcal{R}:V_h^q\to C^2[0,1]\cap V_h^{q+3}$ satisfying*

$$\begin{aligned}(\mathcal{R}(u))_{xxx}&=\mathcal{D}^3u,\\ (\mathcal{R}(u))(x_m^+)&=\{u\}_m,\\ (\mathcal{R}(u))_x(x_m^+)&=\{v_h\}_m,\quad v_h:=\mathcal{D}u,\\ (\mathcal{R}(u))_{xx}(x_m^+)&=\{w_h\}_m,\quad w_h:=\mathcal{D}v_h,\end{aligned} \tag{4.1}$$

with the last three constraints holding for $m=0,\cdots,M-1$.

Proof. The existence of $\mathcal{D}^3u$ being obvious, let us denote it by ψ_h. Now let $\sigma=\mathcal{R}(u)\in V_h^{q+3}$ be the third antiderivative of ψ_h. The three constants generated from the integration can now be chosen so that the last three constraints in (4.1) are satisfied.

It remains to show that σ belongs to $C^2[0,1]$. For a fixed $I=[x_m,x_{m+1}]$, $m=0,\cdots,M-1$, let χ denote the characteristic function of I, we have

$$(\sigma_{xxx},\chi)_I=\sigma_{xx}(x_{m+1}^-)-\sigma_{xx}(x_m^+). \tag{4.2}$$

On the other hand, note that by definition,

$$(\mathcal{D}^3u,\chi)=(\mathcal{D}w_h,\chi)=-(w_h,\chi_x)_I-\sum_{j=0}^{M-1}\{w_h\}_j[\chi]_j=-\{w_h\}_m+\{w_h\}_{m+1}. \tag{4.3}$$

Now the fourth equation of (4.1) stipulates that $\sigma_{xx}(x_m^+)=\{w_h\}_m$ for each m in the range $0,\cdots,M-1$. Hence comparing (4.2) and (4.3) we obtain

$$\sigma_{xx}(x_{m+1}^-)=\{w_h\}_{m+1}=\sigma_{xx}(x_{m+1}^+),\quad m=0,\cdots,M-1, \tag{4.4}$$

which shows that σ_{xx} is continuous on $[0,1]$ and also periodic, the latter following from the case $m=M-1$.

To show that σ_x is continuous and periodic, we use the test function $(x-x_m)\chi$. Arguing as above, we obtain

$$h_m\sigma_{xx}(x_{m+1}^-)-\Big(\sigma_x(x_{m+1}^-)-\sigma_x(x_m^+)\Big)=-(w_h,\chi)+h_m\{w_h\}_{m+1}. \tag{4.5}$$

We already showed in (4.4) that $\sigma_{xx}(x_{m+1}^-)=\{w_h\}_{m+1}$. Hence (4.5) simplifies to

$$\sigma_x(x_{m+1}^-)-\sigma_x(x_m^+)=(w_h,\chi). \tag{4.6}$$

Since $w_h=\mathcal{D}v_h$, it follows that

$$(w_h,\chi)=-\{v_h\}_m+\{v_h\}_{m+1}. \tag{4.7}$$

Using this in (4.6) and the third equation of (4.1) it follows that

$$\sigma_x(x_{m+1}^-)=\{v_h\}_{m+1}=\sigma_x(x_{m+1}^+), \tag{4.8}$$

which shows that σ_x is continuous and periodic.

Finally, to show that σ is also continuous and periodic, we use the test function $(x-x_m)^2\chi$. In this case we obtain

$$h_m^2\sigma_{xx}(x_{m+1}^-)-2h_m\sigma_x(x_{m+1}^-)+2\sigma(x_{m+1}^-)-2\sigma(x_m^+)=-2(w_h,(x-x_m)\chi)+h_m^2\{w_h\}_{m+1},$$

which in view of (4.4) gives

$$h_m\sigma_x(x_{m+1}^-)-\sigma(x_{m+1}^-)+\sigma(x_m^+)=(w_h,(x-x_m)\chi).$$

Using the latter identity and the facts that $w_h=\mathcal{D}v_h$ and $v_h=\mathcal{D}u$, we obtain

$$\begin{aligned}h_m\sigma_x(x_{m+1}^-)-\sigma(x_{m+1}^-)+\sigma(x_m^+)&=-(v_h,\chi)+h_m\{v_h\}_{m+1}\\&=-(\mathcal{D}u,\chi)+h_m\{v_h\}_{m+1}\\&=\{u\}_m-\{u\}_{m+1}+h_m\{v_h\}_{m+1}.\end{aligned}$$

It follows from (4.8) and the second equation of (4.1) that $\sigma(x_{m+1}^-)$ is equal to $\{u\}_{m+1}$ which again in view of the second equation of (4.1) is equal to $\sigma(x_{m+1}^+)$. This concludes the proof of the theorem. □

Remark 4.1. The construction of σ is local to each cell $I\in\mathcal{T}_h$ and proceeds along the lines outlined in [21]. In particular, the coefficients of $\sigma|_I$ in terms of the Legendre polynomials are given as the solution of a linear system with a $(q+4)\times(q+4)$ upper triangular matrix which happens to be independent of I.

4.1 A posteriori estimate for the semidiscrete approximation

We let $\sigma = \mathcal{R}u_h$ denote the reconstruction of the semidiscrete approximation u_h according to Theorem 4.1 above. We readily have

$$\sigma_{xxx} = \mathcal{D}^3 u_h = \mathcal{D} w_h.$$

Hence, from the semidiscrete equation $u_{ht} + \mathcal{N}(u_h) + \epsilon \mathcal{D} w_h = 0$ we have

$$\sigma_t + (\sigma^{p+1})_x + \epsilon \sigma_{xxx} = \sigma_t - u_{ht} + (\sigma^{p+1})_x - \mathcal{N}(u_h) := \eta. \tag{4.9}$$

Note that η is a computable function and more importantly, that (4.9) holds in the strong sense, i.e. pointwise except at the spatial nodes. This makes it possible to prove the following a posteriori estimate for the GKdV equation:

Theorem 4.2. *Let σ and η be defined as above and let $e = \sigma - u$ where u is the solution of the GKdV equation. We have*

$$\|e(t)\|^2 \le e^{ct} \Big(\|e(0)\|^2 + \int_0^t e^{-c\tau} \|\eta(\tau)\|^2 d\tau \Big), \tag{4.10}$$

where the constant c depends on σ and u.

Proof. Comparing this to the GKdV equation, we get

$$e_t + (\sigma^{p+1})_x - (u^{p+1})_x + \epsilon e_{xxx} = \eta. \tag{4.11}$$

Multiplying (4.11) with e and integrating with respect to x, we obtain in view of the periodic boundary conditions

$$\frac{1}{2} \frac{d}{dt} \|e(t)\|^2 - (\psi, e_x) = (\eta, e) \le \frac{1}{2} \|\eta\|^2 + \frac{1}{2} \|e\|^2, \tag{4.12}$$

where $\psi := \sigma^{p+1} - u^{p+1}$. Now observe that

$$(\psi, e_x) = \Big(e \sum_{j=0}^{p} \sigma^{p-j} u^j, e_x \Big) = -\frac{1}{2} \Big(\Big(\sum_{j=0}^{p} \sigma^{p-j} u^j \Big)_x, e^2 \Big) \le \frac{1}{2} c \|e\|^2, \tag{4.13}$$

where c depends on $\|\sigma\|_{W^{1,\infty}}$ and $\|u\|_{W^{1,\infty}}$. Using this estimate in (4.12), the desired estimate (4.10) can be obtained by using the Gronwall's lemma. □

4.2 A posteriori error estimates for a fully discrete scheme

The approach we will follow in deriving a posteriori error estimates for fully discrete approximations is to form a pair of two time-stepping schemes. The first is used to generate the fully discrete approximations and the second to supply the estimation. The difficulty here resides mainly in the fact that fully discrete approximations are indeed discrete whereby there is a need for a function which is continuous in time and satisfies the same differential equation as (1.1) with a computable right hand side.

Let $0\le t^0<t^1<\cdots<t^N=T$ be a partition of the interval $[0,T]$ and $\kappa_n=t^{n+1}-t^n$. The fully discrete approximations u^n to $u(\cdot,t^n)$ generated by the Implicit Euler method are given by

$$u^{n+1}-u^n+\kappa_n\mathcal{N}(u^{n+1})+\kappa_n\epsilon\mathcal{D}w^{n+1}=0, \tag{4.14}$$

$$w^{n+1}=\mathcal{D}v^{n+1},\quad v^{n+1}=\mathcal{D}u^{n+1}, \tag{4.15}$$

which is equivalent to

$$u^{n+1}-u^n+\kappa_n\mathcal{N}(u^{n+1})+\kappa_n\epsilon\mathcal{D}^3u^{n+1}=0, \tag{4.16}$$

with $u^0:=u_h(0)$.

In order to estimate the errors of the Implicit Euler method we will use, at every step, the Midpoint rule which is given by

$$u_M^{n,1}-u^n+\frac{\kappa_n}{2}\mathcal{N}(u_M^{n,1})+\frac{\kappa_n}{2}\epsilon\mathcal{D}w_M^{n,1}=u_M^{n,1}-u^n+\frac{\kappa_n}{2}\mathcal{N}(u_M^{n,1})+\frac{\kappa_n}{2}\epsilon\mathcal{D}^3u_M^{n,1}=0, \tag{4.17}$$

$$u_M^{n+1}=2u_M^{n,1}-u^n,\quad w_M^{n,1}=\mathcal{D}v_M^{n,1},\quad v_M^{n,1}=\mathcal{D}u_M^{n,1}. \tag{4.18}$$

Note that we are using the same value u^n generated by the Implicit Euler method as initial value for the Midpoint rule and we are using the subscript M for the approximations generated by the Midpoint rule.

That both of these schemes are well defined can be established by using a variant of Brouwer's fixed point theorem (cf. [4]). Uniqueness and convergence can be proved under appropriate CFL type conditions.

In addition, the convergence rates

$$\|u(\cdot,t^n)-u^n\|=\mathcal{O}(h^q+\kappa),\quad \kappa=\max_{0\le n\le N}\kappa_n,$$

can be obtained, for details see [4,19].

To derive a posteriori estimates for these schemes we combine ideas of [2,21] and of the semidiscrete case considered previously. Notice first that we make the simplifying assumption that the finite element spaces do not change with time. The general case can be treated also along the lines of [21] but we do not insist on this in the present paper.

The fully discrete reconstruction is defined as the function $\hat{U}:[0,T]\to C^2[0,1]\cap V_h^{q+3}$ which on each interval $I_n=[t^n,t^{n+1}]$ is given by

$$\hat{U}(t)=\mathcal{R}\Big[u^n+\int_{t^n}^t F(s)ds\Big], \tag{4.19}$$

here $F(\cdot)$ is the affine in t function given by

$$F(t)=-\ell_{1/2}(t)\Big\{\mathcal{N}(u_M^{n,1})+\epsilon\mathcal{D}^3u_M^{n,1}\Big\}-\ell_1(t)\Big\{\mathcal{N}(u^{n+1})+\epsilon\mathcal{D}^3u^{n+1}\Big\}, \tag{4.20}$$

where $\ell_{1/2}(t)$ and $\ell_1(t)$ are the two basis functions of the space of affine functions in t on I_n corresponding to the nodes $t^{n,1} := (t^n + t^{n+1})/2$ and t^{n+1} respectively. More specifically

$$\ell_{1/2}(t) = -\frac{2}{\kappa_n}(t - t^{n+1}), \quad \ell_1(t) = \frac{2}{\kappa_n}(t - t^{n,1}).$$

Notice that $\hat{U}$ is a computable piecewise polynomial function. Furthermore, the next lemma shows that it is related to the continuous in t function $U(t) = \big((t^{n+1} - t)u^n + (t - t^n)u^{n+1}\big)/\kappa_n$, i.e. the affine interpolant of the nodal values u^n and u^{n+1}.

Lemma 4.1. *Let $U(t)$ be given as above. Then*

$$\hat{U}(t) = \mathcal{R}\Big\{U(t) + \Big[\frac{3}{4}\hat{\ell}_{1/2}(t) + \hat{\ell}_1(t)\Big]\big(u_M^{n+1} - u^{n+1}\big)\Big\}, \tag{4.21}$$

where the quadratic functions $\hat{\ell}_{1/2}(t)$ and $\hat{\ell}_1(t)$ are given by

$$\hat{\ell}_{1/2}(t) = -\frac{4}{\kappa_n^2}(t - t^n)(t - t^{n+1}), \quad \hat{\ell}_1(t) = \frac{2}{\kappa_n^2}(t - t^n)(t - t^{n,1}).$$

Proof. Since $F(t)$ is affine, and the midpoint rule of quadrature is exact for such functions, from (4.19), (4.20) and (4.17) we obtain

$$\begin{aligned}
\hat{U}(t^{n+1}) &= \mathcal{R}\left\{u^n + \int_{t^n}^{t^{n+1}} F(s)\,ds\right\} = \mathcal{R}\left\{u^n + \kappa_n F(t^{n,1})\right\} \\
&= \mathcal{R}\left\{u^n - \kappa_n\big(\mathcal{N}(u_M^{n,1}) + \epsilon\mathcal{D}^3 u_M^{n,1}\big)\right\} = \mathcal{R}u_M^{n+1} \\
&= \mathcal{R}\{u^{n+1}\} + \mathcal{R}\{u_M^{n+1} - u^{n+1}\}.
\end{aligned} \tag{4.22}$$

Also, since $\ell_{1/2}(t^n) = 2$, $\ell_1(t^n) = -1$, $\ell_{1/2}(t^{n,1}) = 1$, $\ell_1(t_{n,1}) = 0$ and the trapezoidal rule is exact for affine functions, we obtain from (4.17) and (4.14)

$$\begin{aligned}
\hat{U}(t^{n,1}) &= \mathcal{R}\left\{u^n + \frac{\kappa_n}{4}\Big[F(t^n) + F(t^{n,1})\Big]\right\} \\
&= \mathcal{R}\left\{u^n - \frac{\kappa_n}{4}\Big[3\Big(\mathcal{N}(u_M^{n,1}) + \epsilon\mathcal{D}^3 u_M^{n,1}\Big) - \Big(\mathcal{N}(u^{n+1}) + \epsilon\mathcal{D}^3 u^{n+1}\Big)\Big]\right\} \\
&= \mathcal{R}\left\{\frac{1}{2}u^n + \frac{3}{4}u_M^{n+1} - \frac{1}{4}u^{n+1}\right\} = \mathcal{R}\left\{\frac{1}{2}(u^n + u^{n+1}) + \frac{3}{4}(u_M^{n+1} - u^{n+1})\right\} \\
&= \mathcal{R}\left\{U(t^{n,1}) + \frac{3}{4}(u_M^{n+1} - u^{n+1})\right\}.
\end{aligned} \tag{4.23}$$

Finally, since $\hat{U}(t^n) = \mathcal{R}u^n = \mathcal{R}U(t^n)$, the result (4.21) follows from (4.22) and (4.23) and the fact that $\tilde{\ell}_{1/2}(t)$ and $\tilde{\ell}_1(t)$ are the Lagrange basis functions corresponding to the points $t^{n,1}$ and t^{n+1} respectively. ☐

We next derive an error equation for $\rho(t) := \hat{U}(t) - u(t)$.

Lemma 4.2. *$\rho(t)$ satisfies*

$$\rho_t + \big(\hat{U}^{p+1}\big)_x - \big(u^{p+1}\big)_x + \epsilon \rho_{xxx} = \mathcal{E}_1 + \mathcal{E}_2 + \mathcal{E}_3, \tag{4.24}$$

where the error indicators $\mathcal{E}_1, \mathcal{E}_2, \mathcal{E}_3$ are given by

$$\mathcal{E}_1 = \big(\hat{U}^{p+1}\big)_x - \mathcal{R}\Big\{\ell_{1/2}(t)\mathcal{N}\big(u_M^{n,1}\big) + \ell_1(t)\mathcal{N}\big(u^{n+1}\big)\Big\}, \tag{4.25}$$

$$\mathcal{E}_2 = \epsilon\big(I - \mathcal{R}\big)\mathcal{D}^3\Big(U(t) + \frac{1}{2}\ell_{1/2}(t)\big(u_M^{n+1} - u^{n+1}\big)\Big), \tag{4.26}$$

$$\mathcal{E}_3 = \epsilon\left[\frac{3}{4}\hat{\ell}_{1/2}(t) + \hat{\ell}_1(t) - \frac{1}{2}\ell_{1/2}(t)\right]\mathcal{D}^3\big(u_M^{n+1} - u^{n+1}\big). \tag{4.27}$$

Proof. From the definitions of $F(t)$ and $U(t)$ we have

$$\begin{aligned}
\hat{U}_t = \mathcal{R}F(t) &= -\mathcal{R}\Big\{\ell_{1/2}(t)\big(\mathcal{N}(u_M^{n,1}) + \epsilon\mathcal{D}^3 u_M^{n,1}\big) + \ell_1(t)\big(\mathcal{N}(u^{n+1}) + \epsilon\mathcal{D}^3 u^{n+1}\big)\Big\} \\
&= -\mathcal{R}\Big\{\ell_{1/2}(t)\mathcal{N}(u_M^{n,1}) + \ell_1(t)\mathcal{N}(u^{n+1}) + \epsilon\mathcal{D}^3 U(t) + \frac{1}{2}\epsilon\ell_{1/2}(t)\mathcal{D}^3\big(u_M^{n+1} - u^{n+1}\big)\Big\},
\end{aligned} \tag{4.28}$$

where we have used the linearity of the operator $\mathcal{D}$. On the other hand, from (4.21) it follows that

$$\hat{U}_{xxx}(t) = \mathcal{D}^3 U(t) + \left[\frac{3}{4}\hat{\ell}_{1/2}(t) + \hat{\ell}_1(t)\right]\mathcal{D}^3\big(u_M^{n+1} - u^{n+1}\big). \tag{4.29}$$

Combining (4.28) and (4.29), adding $\big(\hat{U}^{p+1}\big)_x$ to both sides and using (1.1) we obtain (4.24). ☐

The next result provides the a posteriori estimate for the fully discrete scheme generated by the Backward Euler scheme (4.14). In doing so we also define the error indicator

$$\mathcal{E}_4^n = \frac{1}{\sqrt{\kappa_n}}\Big(\hat{U}(t^n) - \hat{U}(t^{n-})\Big) = -\frac{1}{\sqrt{\kappa_n}}\Big(\mathcal{R}\big(u_M^n - u^n\big)\Big), \quad n = 1,2,\cdots, \tag{4.30}$$

which appears due to the fact that the function $\hat{U}(t)$ is discontinuous at the temporal nodes $t^1, \cdots, t^{N-1}$.

Theorem 4.3. *Let u^n be the solution of the fully discrete scheme* (4.14)*, and let $\hat{U}$ the discrete reconstruction defined by* (4.19)*. With the error indicators $\mathcal{E}_1, \mathcal{E}_2, \mathcal{E}_3, \mathcal{E}_4$ given by* (4.25), (4.26), (4.27) *and* (4.30)*, there holds the a posteriori error estimate*

$$\|u(t^n) - u^n\| \le \|u^n - \mathcal{R}u^n\| + c e^{ct^n}\left(\|u^0 - \mathcal{R}u^0\|^2 + \sum_{i=1}^{3}\int_0^{t^n}\|\mathcal{E}_i(s)\|^2 ds + \sum_{j=1}^{n}\|\mathcal{E}_4^j\|^2\right)^{1/2}, \tag{4.31}$$

where c is a constant that depends only on u and $\hat{U}$.

Proof. Letting $\mathcal{E}:=\mathcal{E}_1+\mathcal{E}_2+\mathcal{E}_3$, multiplying both sides of (4.24) by ρ and integrating with respect to x gives

$$\frac{1}{2}\frac{d}{dt}\|\rho(t)\|^2+\Big(\big(\hat{U}^{p+1}\big)_x-\big(u^{p+1}\big)_x,\rho(t)\Big)=\big(\mathcal{E}(t),\rho(t)\big),\quad t^n\le t\le t^{n+1}. \tag{4.32}$$

We would like to use Gronwall's Lemma. However, we have to deal with the complication arising from the fact that $\hat{U}$ and thus ρ has jumps at $t^1,\cdots,t^{N-1}$. Now as done in the semidiscrete case, we have the bound

$$\Big|\Big(\big(\hat{U}^{p+1}\big)_x-\big(u^{p+1}\big)_x,\rho(t)\Big)\Big|=\frac{1}{2}\Big|\sum_{j=0}^{p}\big((u^j\rho^{p-j})_x,\rho^2\big)\Big|\le c\|\rho(t)\|^2, \tag{4.33}$$

where c depends on the $\max_{t^n\le t\le t^{n+1}}\|u(t)\|_{1,\infty}$ and $\max_{t^n\le t\le t^{n+1}}\|\hat{U}(t)\|_{1,\infty}$. Thus integrating (4.32) from t^n to $t\in[t^n,t^{n+1}]$ and using the arithmetic-geometric mean inequality, we obtain

$$\|\rho(t)\|^2\le\|\rho(t^n)\|^2+c\int_{t^n}^{t}\|\rho(s)\|^2ds+c\int_{t^n}^{t}\|\mathcal{E}(s)\|^2ds. \tag{4.34}$$

From the mean value theorem for integrals we obtain,

$$\max_{t^n\le t\le t^{n+1}}\|\rho(t)\|^2\le(1+c\kappa_n)\left(\|\rho(t^n)\|^2+c\int_{t^n}^{t^{n+1}}\|\mathcal{E}(s)\|^2ds\right). \tag{4.35}$$

In particular, we have

$$\|\rho(t^{n+1-})\|^2\le(1+c\kappa_n)\left(\|\rho(t^n)\|^2+c\int_{t^n}^{t^{n+1}}\|\mathcal{E}(s)\|^2ds\right). \tag{4.36}$$

Now, since u is a smooth function of t, we have

$$\|\rho(t^n)\|^2-\|\rho(t^{n-})\|^2=\big(\hat{U}(t^n)-\hat{U}(t^{n-}),\rho(t^n)+\rho(t^{n-})\big), \tag{4.37}$$

from which we easily obtain

$$\|\rho(t^n)\|^2\le(1+c\kappa_n)\Big(\|\rho(t^{n-})\|^2+\frac{1}{\kappa_n}\|\hat{U}(t^n)-\hat{U}(t^{n-})\|^2\Big). \tag{4.38}$$

Using (4.38) in (4.36) and a discrete version of Gronwall's Lemma, we obtain

$$\max_{0\le t\le T}\|\rho(t)\|^2\le ce^{cT}\Big(\|\rho(0)\|^2+\sum_{n=1}^{N}\frac{1}{\kappa_n}\|\hat{U}(t^n)-\hat{U}(t^{n-})\|^2+\int_0^T\|\mathcal{E}(s)\|^2ds\Big). \tag{4.39}$$

The conclusion now follows from the triangle inequality and the observation that $\hat{U}(t^n)=\mathcal{R}u^n$. $\square$

5 Numerical experiments

In this section, we provide some numerical results to demonstrate the performance of our LDG methods. We will validate the theoretical results including a study of the a priori convergence rates, and compare the performance of the conservative methods to the dissipative LDG methods. We will also study the a posteriori error estimate and experimental confirmation of the a posteriori upper bound.

In these numerical experiments, we consider the following KdV-equation

$$u_t+uu_x+\epsilon u_{xxx}=0 \tag{5.1}$$

with $\epsilon=1/24^2$. The computational domain is set to $[0,1]$, and divided into M cells. To check accuracy and convergence rates, we use the well-known *cnoidal-wave* solution,

$$u(x,t)=a\mathrm{cn}^2(4K(x-vt-x_0)), \tag{5.2}$$

where $cn(z)=cn(z:m)$ is the Jacobi elliptic function with modulus $m=0.9$. The other parameters have the values $a=192m\epsilon K(m)^2$, $v=64\epsilon(2m-1)K(m)^2$ and $x_0=0.5$, where the function $K=K(m)$ is the complete elliptic integral of the first kind and the parameters are so organized that the solution u has spatial period 1. As an alternative, we also consider the classical *solitary-wave* solutions

$$u(x,t)=A\mathrm{sech}^2(K(x-vt-x_0)) \tag{5.3}$$

with the parameters $A=1$, $v=A/3$, $K=\frac{1}{2}\sqrt{\frac{A}{3\epsilon}}$ and $x_0=0.5$. This traveling wave is also a stable solution of the KdV-equation (see [7] and [8] for the original proof of this fact). Of course, the solitary-wave solution is not periodic in space, but it can be treated as periodic by simply restricting it to the computational domain $[0,1]$ and imposing periodic boundary conditions across $x=0$ and $x=1$, thanks to the exponential decay of the hyperbolic secant function.

5.1 A priori convergence rates

In the numerical experiments to test a priori convergence rate, we use the second order midpoint rule time discretization (4.17), which can be shown to be conservative in time. Since our interest is in the effect of the various spatial discretizations, we use $\kappa=h$ when $q=0$, 1, and $\kappa=10h^2$ when $q=2$, 3. The numerical results of conservative LDG methods at time $T=1$ with $q=0,1,2$ are given in Table 1. The L^2- and L^∞-norms of this error are calculated numerically and reported in the tables. We can easily observe the optimal convergence rates for even q, and sub-optimal convergence rates for odd q. In Tables 2 and 3, we show the numerical errors at a longer time, $T=25$, and compare the results with those of dissipative LDG methods of Xu and Shu [27] for even q. From these, we can observe an improved long time behavior of the conservative methods.

Table 1: The accuracy test for the Cnoidal-wave problem, uniform mesh at $T=1$.

	M	κ	L^2 error	order	L^∞ error	order
$q=0$	10	1.0E-01	9.8240E-01		1.8778E-00	
	20	5.0E-02	4.7798E-01	1.0624	1.2235E-00	0.6181
	40	2.5E-02	1.2554E-01	1.9288	4.2038E-01	1.5412
	80	1.25E-02	4.5836E-02	1.4536	1.5092E-01	1.4779
	160	6.25E-03	1.8745E-02	1.2900	5.9854E-02	1.3343
	320	3.125E-03	8.8674E-02	1.0799	2.6272E-02	1.1879
$q=1$	10	1.0E-01	7.3395E-01		1.8675E-00	
	20	5.0E-02	5.9167E-01	0.3109	1.5015E-00	0.3147
	40	2.5E-02	3.6048E-01	0.7149	8.4908E-01	0.8224
	80	1.25E-02	1.9077E-02	0.9181	4.4073E-01	0.9460
	160	6.25E-03	9.7571E-02	0.9673	1.9895E-01	1.1475
	320	3.125E-03	4.9131E-02	0.9898	9.4892E-02	1.0681
$q=2$	10	1.0E-01	8.5400E-01		1.5215E-00	
	20	5.0E-02	3.8071E-02	4.4875	7.8369E-02	4.2791
	40	2.5E-02	2.2880E-03	4.0565	4.5594E-03	4.1034
	80	1.25E-02	1.4724E-04	3.9578	3.2118E-04	3.8274
	160	6.25E-03	9.5960E-06	3.9396	2.6205E-05	3.6154

Table 2: Cnoidal-wave problem, $q=0$, uniform mesh at $T=25$.

	M	κ	L^2 error	order	L^∞ error	order
Conservative method	10	1.0E-01	1.1819E-00		1.8867E-00	
	20	5.0E-02	1.0092E-00	0.2279	1.7589E-00	0.1012
	40	2.5E-02	1.3056E-00	-0.3715	2.0215E-00	-0.2008
	80	1.25E-02	6.3522E-01	1.0394	1.1258E-00	0.8445
	160	6.25E-03	1.6881E-01	1.9119	3.3245E-01	1.7597
	320	3.125E-03	4.2999E-02	1.9730	9.5225E-02	1.8037
Dissipative method	10	1.0E-01	6.9103E-01		1.2519E-00	
	20	5.0E-02	6.9103E-01	0.0000	1.2659E-00	-0.0160
	40	2.5E-02	6.9103E-01	0.0000	1.2660E-00	-0.0002
	80	1.25E-02	6.9103E-01	0.0000	1.2661E-00	-0.0001
	160	6.25E-03	6.9103E-01	0.0000	1.2661E-00	-0.0001
	320	3.125E-03	6.9199E-01	-0.0020	1.2675E-00	-0.0016

5.2 Comparison of the conservative and dissipative methods

In this subsection, we have included further numerical results to acquire a deeper understanding of the performance of the conservative and dissipative numerical methods.

Table 3: Cnoidal-wave problem, $q=2$, uniform mesh at $T=25$.

	M	κ	L^2 error	order	L^∞ error	order
Conservative method	10	1.0E-01	9.1479E-01		1.5849E-00	
	20	2.5E-02	8.4871E-01	0.1082	1.3908E-00	0.1885
	40	6.25E-03	4.7032E-02	4.1736	7.9666E-02	4.1258
	80	1.5625E-03	3.6080E-03	3.7044	6.1220E-03	3.7019
	160	3.90625E-04	2.2688E-04	3.9912	3.8968E-04	3.9736
Dissipative method	10	1.0E-01	8.9741E-01		1.5296E-00	
	20	2.5E-02	1.2202E-00	-0.4433	1.8738E-00	-0.2928
	40	6.25E-03	1.4977E-01	3.0263	2.5260E-01	2.8910
	80	1.5625E-03	6.9580E-03	4.4279	1.1767E-02	4.4241
	160	3.90625E-04	3.3520E-04	4.3756	5.7521E-04	4.3545

A graphical approach is adopted to demonstrate behavior that may not be revealed by simple tabulation of convergence rates.

We start with the cnoidal-wave test problem with $q=0$ and $\kappa=0.01$. Fig. 1 shows the plots of the numerical solutions of the proposed conservative and dissipative methods at time $t=25$ with different mesh size. The exact solution is also provided as a reference in the plot. The numerical dissipative methods have a large error, and the wave is damped to almost zero even with refined 640 meshes.

Next, quadratic polynomials with $q=2$ are tested. We repeat the same test as above with $M=20$ and the same κ. The comparison of numerical solutions at time $T=25$ is shown in Fig. 2, left, where the large phase errors of dissipative methods can be easily observed. The same test with $M=40$ is repeated, and shown in Fig. 2, middle, where the dissipative methods have a much improved performance on the refined mesh. However, when we ran this test for longer, until $T=50$, we observed the larger phase errors again in the approximation made via the dissipative method, as shown in the right graph of Fig. 2.

5.3 A posteriori error convergence rate

In this subsection, we show the numerical experiments which are devoted to studying the behavior of the various quantities appearing in Theorem 4.3. Both the backward Euler method (4.16) and the midpoint rule time discretization (4.17) are used to derive the a posteriori error indicator. We use the notations

$$\eta_i=\Big(\int_0^{t^n}\|\mathcal{E}_i(t)\|^2 ds\Big)^{1/2},\ i=1,2,3;\quad \eta_4=\Big(\sum_{j=0}^{n}\|\mathcal{E}_4^j\|^2\Big)^{1/2},\quad \eta_{tot}=\Big(\sum_{i=1}^{4}\eta_i^2\Big)^{1/2},$$

and study the decreasing rate of the (total) a posteriori error indicator η_{tot}. In particular we would like to show that it decreases at the rate of $\mathcal{O}(\kappa)$. In order to render very small

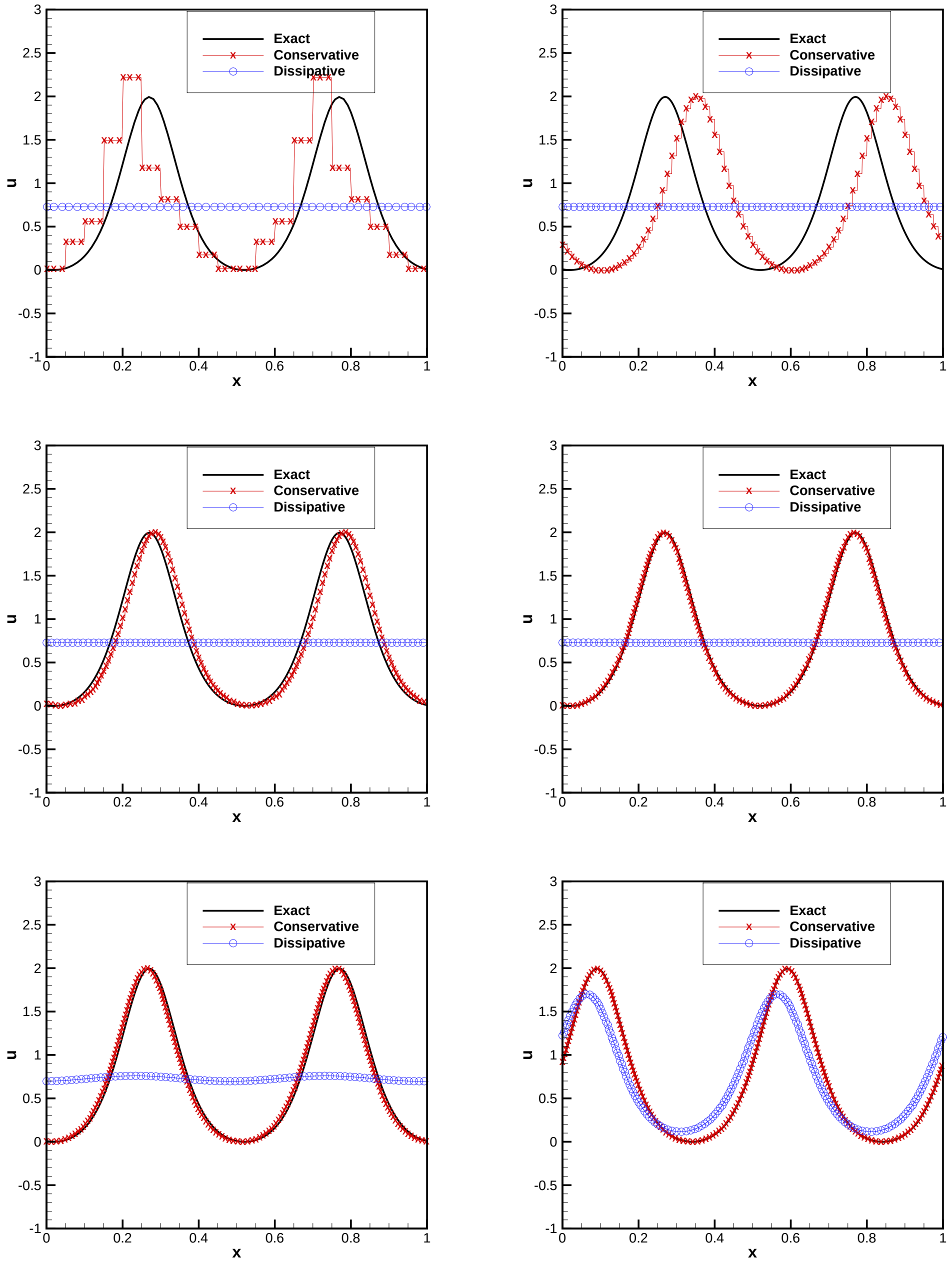

Figure 1: Numerical approximations of the cnoidal-wave problem using the conservative and dissipative methods; comparisons with the exact solution at time $t=25$ (except the last figure) with $q=0$. Top left: 20 cells; Top right: 80 cells; Middle left: 160 cells; Middle right: 320 cells; Bottom left: 640 cells; Bottom right: 640 cells at $T=1$.

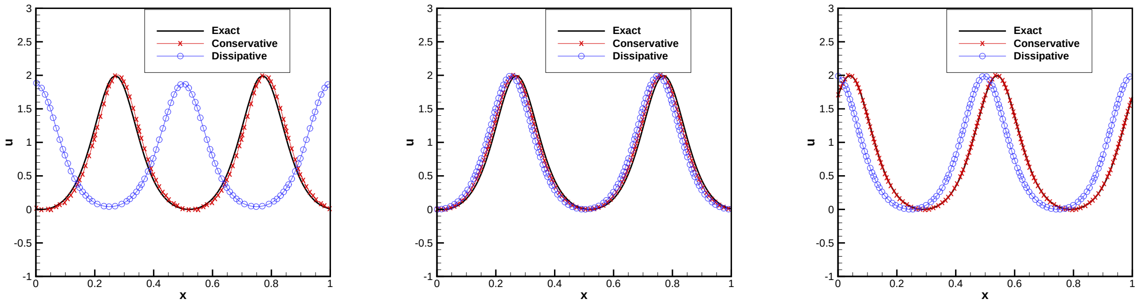

Figure 2: Numerical approximations of the cnoidal-wave problem using the conservative and dissipative methods; comparisons with the exact solution at time $t=25$ with $q=2$. Left: 20 cells at $T=25$; Middle: 40 cells at $T=25$; Right: 40 cells at $T=50$

Table 4: The a posteriori error convergence rate with solitary wave solution, $T=1$, $p=1$, $\epsilon=.0001$, $M=500$, $q=5$.

N	η_1	η_2	η_3	η_4	η_{tot}	rate	$\|u(T)-u^N\|$	rate
100	3.06E-02	1.66E-06	2.63E-02	8.96E-02	9.82E-02		1.88E-01	
200	9.61E-03	1.61E-06	8.07E-03	5.33E-02	5.48E-02	0.841	1.33E-01	0.491
400	2.88E-03	1.68E-06	2.36E-03	3.08E-02	3.10E-02	0.823	8.29E-02	0.687
800	8.17E-04	2.06E-06	6.66E-04	1.69E-02	1.69E-02	0.875	4.67E-02	0.828
1600	2.20E-04	1.99E-06	1.79E-04	8.88E-03	8.88E-03	0.928	2.48E-02	0.913
3200	5.72E-05	1.84E-06	4.67E-05	4.57E-03	4.57E-03	0.958	1.28E-02	0.954

spatial numerical errors, we chose $M=500$ and $q=5$. Table 4 shows the a posteriori error indicator with different time steps N, as well as the decreasing rate of η_{tot} which decrease at the rate of $\mathcal{O}(\kappa)$ as expected. Similar as the observation in [21], we observe that as κ decreases η_4 converges to η_{tot}. This may have practical value in that among all the indicators η_4 is the least expensive to evaluate.

5.4 A posteriori error indicator

In this subsection, we show the time history of the six quantities η_i, $i=1,\cdots,4$, η_{tot} and the L^2 error $\|u(t^n)-u^n\|$, until $T=1$. The numerical results with a larger κ and $N=200$, hence low temporal accuracy, are shown in Fig. 3. Those with a smaller κ and $N=500$, hence higher temporal accuracy, are shown in Fig. 4. We would like to comment that the difference between the sub-linear behavior of η_{tot} and the super-linear behavior of the L^2 error comes from the exponential term on the right hand side of (4.31). From the point of view of effectivity indices, η_{tot} and the actual errors are within a factor of 2 or 3 of each other over the range of integrations considered. The estimator η_3 is relatively large for $q=2$, and stays level. It decays quickly as the polynomial degree q increases. Out of four

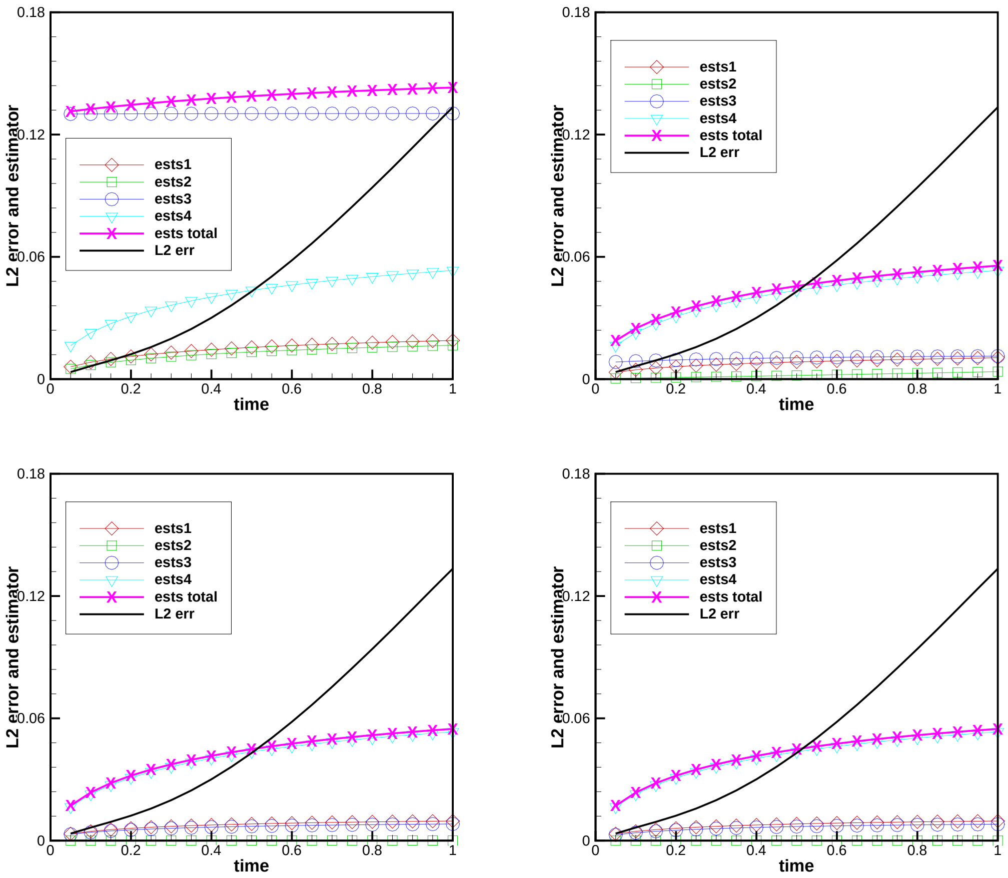

Figure 3: A posteriori approximations of the Solitary wave with $A=1$, $p=1$, $\epsilon=10^{-4}$, $M=200$, $N=200$, $T=1$. Top left: $q=2$, top right: $q=3$, bottom left: $q=4$, bottom right: $q=5$.

η estimator, the dominating one is again η_4. Since η_4 is the least expensive error indicator, further investigation will be carried out to test a heuristic of using only η_4 as the indicator. Other future work includes the extensions to higher order temporal discretizations and the treatment of other nonlinear dispersive equations possessing higher order spatial derivatives.

Acknowledgments

The research of O. Karakashian was partially supported by National Science Foundation grant DMS-1216740. The research of Y. Xing was partially supported by National Science Foundation grants DMS-1216454 and DMS-1621111.

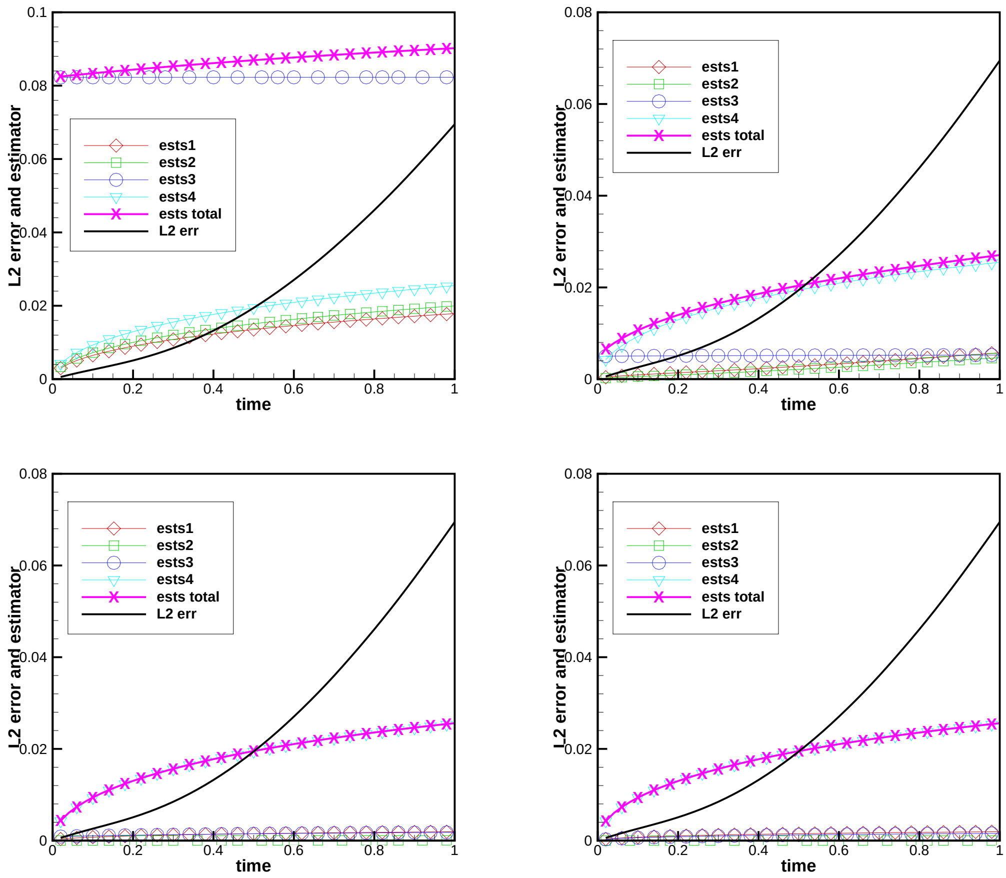

Figure 4: A posteriori approximations of the Solitary wave with $A=1$, $p=1$, $\epsilon=10^{-4}$, $M=200$, $N=500$, $T=1$. Top left: $q=2$, top right: $q=3$, bottom left: $q=4$, bottom right: $q=5$.

References

[1] R. Adams. *Sobolev Spaces*. Academic Press, New York, 1975.

[2] G. Akrivis, C. Makridakis, and R. H. Nochetto. A posteriori error estimates for the Crank–Nicolson method for parabolic equations. *Math. Comp.*, 75:511–531, 2006.

[3] J. Angulo, J.L. Bona, F. Linares, and M. Scialom. Scaling, stability and singularities for nonlinear dispersive wave equations: The critical case. *Nonlinearity*, 15:759–786, 2002.

[4] G. Baker, V.A. Dougalis, and O.A. Karakashian. Convergence of Galerkin approximations for the Korteweg-de Vries equation. *Math. Comp.*, 40:419–433, 1983.

[5] G. Baker, W. Jureidini, and O.A. Karakashian. Piecewise solenoidal vector fields and the Stokes problem. *SIAM J. Num. Anal.*, 27:1466–1485, 1990.

[6] F. Bassi and S. Rebay. A high-order accurate discontinuous finite element method for the numerical solution of the compressible Navier-Stokes equations. *J. of Comput. Phys.*, 131:267–279, 1997.

[7] T.B. Benjamin. The stability of solitary waves. *Proc. Royal Soc. London, Ser. A*, 328:153–183, 1972.

[8] J.L. Bona. On the stabilty theory of solitary waves. *Proc. Royal Soc. London, Ser. A*, 349:363–374, 1975.

[9] J.L. Bona, H. Chen, O. Karakashian, and Y. Xing. Conservative discontiuous Galerkin methods for generalized Korteweg-de Vries equation. *Math. Comp.*, 82(283):1401–1432, 2013.

[10] S. Brenner and L.R. Scott. *The Mathematical Theory of Finite Element Methods*, volume 15 of *Texts in Applied Mathematics*. Springer Verlag, New York, third edition, 2002.

[11] Y. Cheng and C.-W. Shu. A discontinuous finite element method for time dependent partial differential equations with higher order derivatives. *Math. Comp.*, 77:699–730, 2008.

[12] Y. Cheng and C.-W. Shu. Superconvergence and time evolution of discontinuous Galerkin finite element solutions. *J. of Comput. Phys.*, 227:9612–9627, 2008.

[13] B. Cockburn, S. Hou, and C.-W. Shu. The Runge-Kutta local projection discontinuous Galerkin finite element method for conservation laws IV: the multidimensional case. *Math. Comp.*, 54:545–581, 1990.

[14] B. Cockburn, S.-Y. Lin, and C.-W. Shu. TVB Runge-Kutta local projection discontinuous Galerkin finite element method for conservation laws III: one dimensional systems. *J. of Comput. Phys.*, 84:90–113, 1989.

[15] B. Cockburn and C.-W. Shu. TVB Runge-Kutta local projection discontinuous Galerkin finite element method for conservation laws II: general framework. *Math. Comp.*, 52:411–435, 1989.

[16] B. Cockburn and C.-W. Shu. The local discontinuous Galerkin finite element method for convection-diffusion systems. *SIAM J. Numer. Anal.*, 35:2440–2463, 1998.

[17] B. Cockburn and C.-W. Shu. The Runge-Kutta discontinuous Galerkin method for conservation laws V: multidimensional systems. *J. of Comput. Phys.*, 141:199–224, 1998.

[18] B. Cockburn and C.-W. Shu. Runge-Kutta discontinuous Galerkin methods for convection-dominated problems. *J. Sci. Comput.*, 16:173–261, 2001.

[19] V.A. Dougalis and O.A. Karakashian. On some high order accurate fully discrete Galerkin methods for the Kortweg-de Vries equation. *Math. Comp.*, 45:329–345, 1985.

[20] C. Hufford and Y. Xing. Superconvergence of the local discontinuous galerkin method for the linearized korteweg-de vries equation. *J. Comput. Appl. Math.*, 255:441–455, 2014.

[21] O. Karakashian and C. Makridakis. A posteriori error estimates for discontinuous galerkin methods for the generalized korteweg-de vries equation. *Math. Comp.*, 84(293):1145–1167, 2015.

[22] O. Karakashian and Y. Xing. On the construction of compatible and optimal-order initial approximations for local discontinuous Galerkin methods. *In preparation*.

[23] Y. Martel and F. Merle. Stability of blow-up profile and lower bounds on the blow up rate for the critical generalized KdV equation. *Annals Math.*, 155:235–280, 2002.

[24] F. Merle. Existence of blow-up solutions in the energy space for the critical generalized KdV equation. *J. American Math. Soc.*, 14:666–678, 2001.

[25] W.H. Reed and T.R. Hill. Triangular mesh methods for the neutron transport equation. Technical Report LA-UR-73-479, Los Alamos Scientific Laboratory, 1973.

[26] C.-W. Shu. Discontinuous Galerkin methods for time-dependent problems: Survey and recent developments. In X. Feng, O. Karakashian, and Y. Xing, editors, *Proceedings of the 2012 John H. Barrett Memorial Lectures: Recent developments in discontinuous Galerkin finite element methods for partial differential equation*, volume 157 of *IMA volumes in Mathematics and its applications*, pages 25–62. Springer, 2014.

[27] Y. Xu and C.-W. Shu. Error estimates of the semi-discrete local discontinuous Galerkin

method for nonlinear convection-diffusion and KdV equations. *Computer Methods in Appl. Mech. and Eng.*, 196:3805–3822, 2007.

[28] Y. Xu and C.-W. Shu. Optimal error estimates of the semi-discrete local discontinuous Galerkin methods for high order wave equations. *SIAM J. Numer. Anal.*, 50:79–104, 2012.

[29] J. Yan and C.-W. Shu. A local discontinuous Galerkin method for KdV type equations. *SIAM J. Numer. Anal.*, 40:769–791, 2002.